NANO LETTERS

XXXX
Vol. xx, No. x
-

Ultrasmall Mode Volume Plasmonic Nanodisk Resonators

Martin Kuttge,*,† F. Javier García de Abajo,‡ and Albert Polman†

Center for Nanophotonics, FOM-Institute AMOLF, Sciencepark 113, 1098 XG Amsterdam, The Netherlands, and Instituto de Óptica - CSIC, Serrano 121, 28006 Madrid, Spain

Received August 5, 2009; Revised Manuscript Received October 1, 2009

ABSTRACT

We study the resonant modes of nanoscale disk resonators sustaining metal−insulator−metal (MIM) plasmons and demonstrate the versatility of these cavities to achieve ultrasmall cavity mode volume. Ag/SiO_2/Ag MIM structures were made by thin-film deposition and focused ion beam milling with cavity diameters that ranged from $d = 65-2000$ nm. High-resolution two-dimensional cavity-mode field distributions were determined using cathodoluminescence imaging spectroscopy and are in good agreement with boundary element calculations. For the smallest cavities ($d = 65-140$ nm), the lowest order mode ($m = 1$, $n = 1$) is observed in the visible spectral range. This mode is of similar nature as the one in plasmonic particle dimers, establishing a natural connection between localized and traveling plasmon cavities. A cavity quality factor of $Q = 16$ is observed for the 105 nm diameter cavity, accompanied by a mode volume as small as $0.00033\lambda_0^3$. The corresponding Purcell factor is 900, making these ultrasmall disk resonators ideal candidates for studies of enhanced spontaneous emission and lasing.

Optical microcavities have been central in enabling control of the light emission in LEDs and lasers for application in quantum optics and telecommunication.[1−3] These applications rely on the effective confinement of light in a small cavity mode volume. While most of the cavity designs so far are based on dielectric material assemblies, the confinement of light using metallic nanostructures has recently become a topic of great interest. In these structures, the optical fields are dominated by surface plasmon polaritons (SPPs), electromagnetic waves bound to the interface between a metal and a dielectric.[4] Particularly strong confinement of light can be achieved in metal−insulator−metal (MIM) geometries in which a 10−100 nm thick insulator layer is sandwiched between two metal films and the lateral extent of the optical fields is thus limited to only tens of nanometers.[5−7]

Even though the one-dimensional propagation of MIM plasmons has been well characterized,[8,9] the confinement of MIM plasmons in resonator structures has not been explored in much detail so far. The combination of ultrathin MIM geometries with the lateral confinement of resonator structures can yield cavities with much smaller mode volumes than what can be achieved with dielectric cavities.

In this letter, we study the plasmonic modes and field confinement of disk-shaped cavities composed of a MIM waveguide core. We use cathodoluminescence (CL) imaging spectroscopy to acquire the resonance spectra and image the modes inside the resonators. For large disks, we find resonator modes that can be characterized in a way similar to dielectric disk resonator modes. For disks with diameters much smaller than the wavelength, we find a single mode, which is essentially electrostatic in nature. The cavity mode volume is derived and is 2−3 orders of magnitudes smaller than in photonic crystal and dielectric cavities. The experimentally measured quality factor for these cavities is $Q = 16$ resulting in a Purcell factor of $F_P = 900$.

The MIM samples were prepared using physical vapor deposition from a thermal evaporation source onto a cleaned silicon substrate. The layer stack consisted of subsequent layers of 10 nm chromium, 100 nm silver, 10 or 50 nm SiO_2, 100 nm silver, and 10 nm chromium. The chromium layers were deposited to damp out SPPs that would otherwise propagate at the Ag/air and Ag/Si interfaces. We used the 30 keV Ga^+ beam of a focused ion beam (FIB) system to carve disk resonator structures into the MIM stack by etching away a 1 μm wide ring. The focused ion beam (beam current 48 nA) etched through the entire layer stack and approximately 200 nm into the underlying silicon substrate. A schematic drawing of the studied structure is presented in Figure 1a. Figure 1b shows a scanning electron micrograph (SEM) image of a disk resonator with a diameter of 2000 nm, imaged under an angle of 52° off the surface normal.

We used spatially resolved cathodoluminescence imaging spectroscopy[10] to excite plasmon modes in the MIM resonators and measure the emission in the far field. The samples were excited by the 30 keV electron beam of an SEM, which

* To whom correspondence should be addressed. E-mail: kuttge@amolf.nl.
† FOM-Institute AMOLF.
‡ Instituto de Óptica - CSIC.

10.1021/nl902546r CCC: $40.75

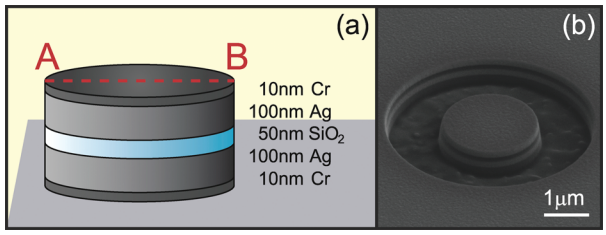

Figure 1. (a) Schematic of a MIM disk resonator. A 10−50 nm thick SiO_2 film is embedded between optically thick Ag films. (b) SEM image of a MIM disk resonator with a diameter of 2000 nm (50 nm thick SiO_2) taken under an angle of 52°.

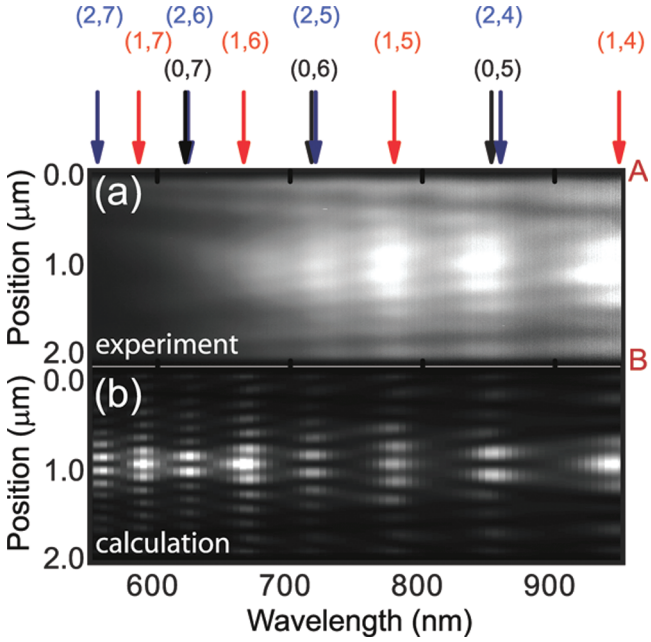

Figure 2. (a) Cathodoluminescence intensity measured as a function of electron beam position and free-space wavelength for a line scan across a $Ag/SiO_2/Ag$ MIM disk resonator with 2000 nm diameter (50 nm SiO_2). (b) CL emission map calculated using BEM for the same structure as in (a). The arrows denote the wavelengths of disk resonator modes with mode numbers (m, n).

was focused to a 10 nm spot onto the sample surface. Because of electron scattering in the upper metal layers, the beam diameter is increased to approximately 50 nm as it penetrates into the silica layer. A parabolic mirror (acceptance angle 1.4π *sr*) placed above the sample collects the light emitted from the sample and guides it to a spectrometer in which the light is spectrally resolved and detected using a liquid-nitrogen-cooled charge-coupled device array. The measured spectra were corrected for system response by measuring the transition radiation spectrum for a known gold sample and normalizing it to the calculated transition radiation spectrum.[10]

Figure 2a shows the measured CL emission as a function of free-space wavelength and electron beam position for a line scan across the center of a disk resonator with a diameter of 2000 nm (running from A to B in Figure 1a). We observe an oscillatory pattern of the CL intensity as a function of wavelength and position of the electron beam. Additionally, five spectral bands of increased emission are observed at wavelengths of 670, 720, 770, 840, and 940 nm. The intensity of these bands decreases for shorter wavelengths due to ohmic losses and absorption the silica.

We attribute these observed bright spectral bands in the spectrum to the excitation of resonant modes inside the disk resonator. To identify the nature of the modes, we have used a model to solve for the modes of dielectric disk cavities.[11] The cavity was modeled by an effective mode index $n_{\mathrm{eff}}(\omega)$, derived from the dispersion relation of planar MIM plasmons. The resonance frequency of the disk modes was then calculated, as well as their azimuthal and radial mode numbers m and n, respectively. The free-space wavelengths corresponding to these modes are indicated by arrows in Figure 2, together with the corresponding mode numbers. For the disk geometry in Figure 1a, we find azimuthal mode numbers of $m = 0,\ 1,\ 2$ and radial mode numbers $n = 4-7$ in the 550−950 nm spectral range. The calculated resonance wavelengths of the modes agree well with the observed bands in the experimental data in Figure 2a. The radial mode numbers indicate the number of antinodes along the radial direction, and are in excellent agreement with the measured pattern in Figure 2a.

While the simple dielectric model can predict the frequency of resonant modes and the mode indices, it cannot yield the spatial field profiles of the cavity modes. To do so, we have solved Maxwell's equations for this system using a boundary-element-method (BEM) for rotationally invariant structures.[12,13] The fields in the BEM calculations can be separated into azimuthal components with a dependence on the azimuthal angle ϕ as $\propto e^{im\phi}$, where m is the azimuthal number (note that m and $-m$ modes are degenerate, and therefore, for simplicity, we refer here to positive values of m only). We have calculated the angle-dependent emission for 30 keV electrons incident on the studied structure and have integrated the emission for azimuthal numbers up to $m = 2$ over the mirror collection angles. Note that due to secondary ion milling the side walls of the resonators are slightly tilted. The resulting conical shape was included in the simulations and was shown to broaden the calculated resonances. The resulting emission distribution as a function of wavelength is shown in Figure 2(b). The oscillatory spatial pattern and the wavelengths of the observed bright bands are in excellent agreement with the experimental data of Figure 2(a).

In order to further visualize the spatial mode patterns, we have calculated the contributions to the CL emission originating from different azimuthal modes. Figure 3 shows the calculated position-dependent emission intensity at the wavelengths of the bright spectral bands observed in Figure 2a, resolved into different mode numbers (m, n) and superimposed with a $\cos^2(m\phi)$ dependence to emphasize the azimuthal dependence of the fields. While the azimuthal mode number is determined by the calculation setting, radial mode numbers can be determined from the number of radial antinodes in the emission pattern. We find that within the experimental spectral range, the BEM-calculated disk resonances are described by radial mode numbers $n = 4-7$, in agreement with the dielectric disk resonator model, thus

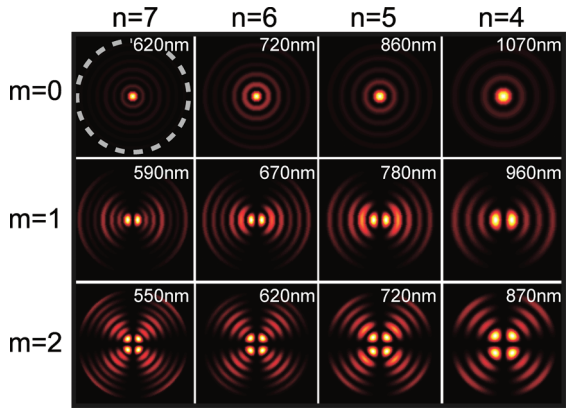

Figure 3. Calculated two-dimensional CL emission maps for a 30 keV electron beam incident onto a Ag/SiO_2/Ag MIM disk resonator with a diameter of 2000 nm (50 nm SiO_2) for different mode numbers (m, n). The images show the dependence of the emission intensity on the position of the electron spot. A $\cos^2(m\phi)$ dependence has been superimposed to the intensity to emphasize the azimuthal dependence of the fields. The central wavelengths of the modes are indicated by text insets. The white dashed circle shows the boundary of the disk.

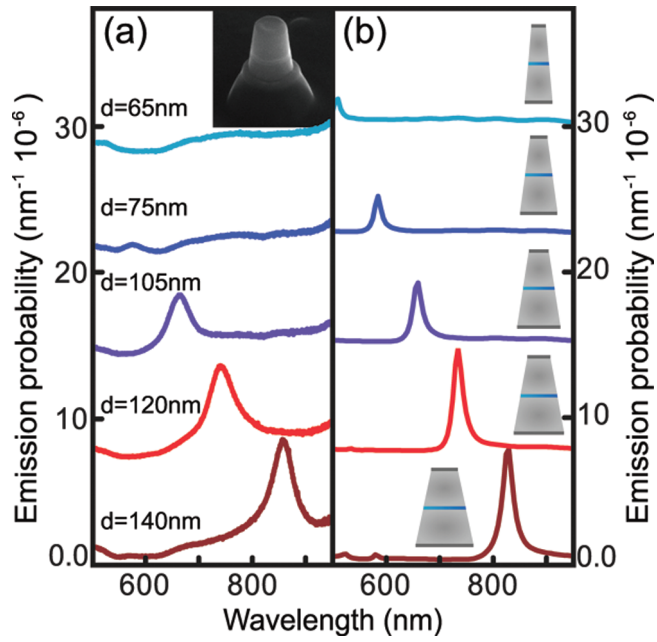

Figure 4. (a) Measured CL spectra for Ag/SiO_2/Ag nanodisk resonators (10 nm SiO_2) with different diameters in the range d = 65−140 nm. (b) Calculated CL spectra for the geometries corresponding to the measurements of (a). Spectra are vertically offset for clarity. The inset in (a) shows an SEM image of a plasmonic nanodisk cavity with d = 65 nm.

confirming that the latter model can be applied to derive the MIM disk cavity mode frequencies.

Because of their large diameter, the disk resonators studied above host a large number of high-order modes. Next, we investigate resonators with smaller dimensions to study the possibility of achieving single-mode cavities with the smallest possible mode volume. To do so, we have reduced the SiO_2 layer thickness from 50 to 10 nm. Using FIB, we have milled resonators out of a Ag/SiO_2/Ag stack with diameters ranging from 65 to 140 nm. Because of secondary ion milling, the resonators have a conical shape with a side wall angle of approximately 7° (see inset in Figure 4).

We have acquired CL spectra by scanning the electron beam quickly over the entire resonator area while detecting the emitted radiation. This procedure was used to prevent electron beam-induced deformation, which occurs when the electron beam is scanned more slowly over these ultrasmall structures. Figure 4a shows the measured CL spectra for five resonators with different disk diameters. A single prominent spectral feature is observed for the three largest cavities (d = 105, 120, 140 nm), that shifts to shorter wavelength for decreasing diameter. For the two smallest disks, a further blue-shifted feature is observed despite being strongly damped. From the dielectric disk resonator model, we can identify the main peak as (m, n) = (1, 1) resonance mode in all five cases.

We have also calculated the CL emission spectra for these small resonators using BEM. The spectra averaged over electron-beam positions swapped along the resonator diameter are shown in Figure 4b. The calculated spectra show only a single peak, as in the experiment, and the resonance wavelength corresponds well with what is observed in the measured CL for the different resonator diameters. Note that for the three largest disks the calculated absolute peak CL intensity also agrees quite well with what is experimentally observed.

The experimental cavity quality factor for the 105 nm diameter disk is Q = 16, while from the BEM calculations we obtain a value of Q = 36. The increased line width for the experimental spectra is attributed to two factors, (1) increased plasmon propagation loss due to scattering from nanoscale roughness of the multilayer structures, and (2) a reduction in the reflection coefficient at the cavity boundaries reducing the cavity feedback due to inhomogeneities at the resonator edges. We observed in calculations that the tilted side wall profile leads to a decrease in cavity quality factor. For example, for the above-mentioned cavity the quality factor decreases from Q = 45 for straight side walls to the Q = 36 for the experimental profile. We note that the quality factor for these 10 nm thick cavities is larger than what is observed for the thicker cavities of Figure 2 (e.g., $Q \approx 10$ for the cavities in Figure 2, data not shown), which we attribute to the higher reflectivity of the cavity edges for thinner dielectric layers, as a result of an increased dielectric discontinuity due to the higher mode index for thinner MIM waveguides.

To further investigate the nature of these ultrasmall lowest-order resonant-plasmonic-nanocavity disk-modes, we have used BEM to calculate the scattering cross section spectrum for a resonator with center diameter of 105 nm, using a p-polarized plane-wave incident along the axis of symmetry. The result is shown in Figure 5a. For comparison, we have also plotted the calculated CL emission spectrum (same data as in Figure 4b). The calculated scattering spectrum agrees very well with the calculated CL spectrum. We find that the peak scattering cross section for this resonator is approximately 5.5 times its geometrical cross section. A two-dimensional plot of the CL emission is shown as the inset

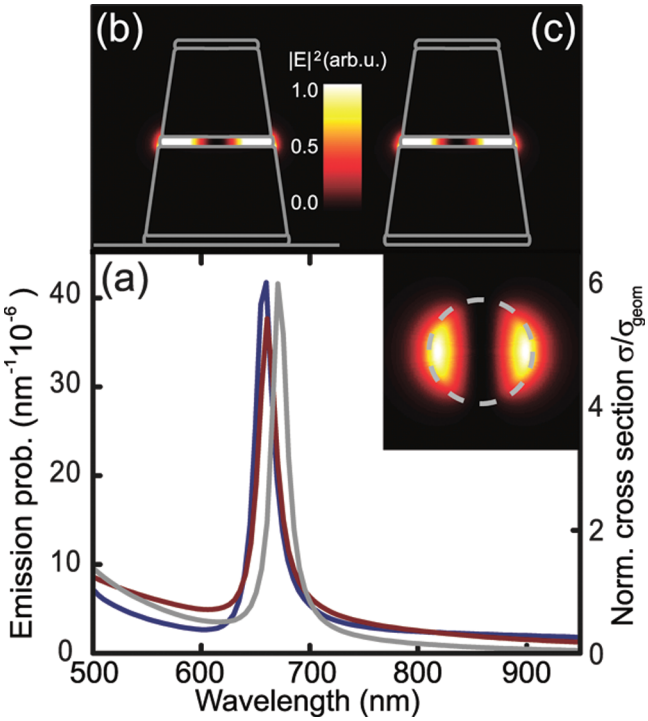

Figure 5. (a) Calculated CL emission spectrum (blue line) for a nanodisk resonator, compared to the calculated scattering cross section of p-polarized light for a nanodisk resonator with (red) and without (gray) chromium capping layers. The cross section is normalized to the projected area of the SiO_2 disk. The inset shows the calculated E_z distribution for the $m = 1$ mode of the 105 nm diameter disk. (b) Calculated electric near-field intensity for a Ag/SiO_2/Ag nanodisk resonator with a central diameter of 105 nm at a wavelength of 660 nm, imaged on a plane containing the symmetry axis of the resonator. The resonator was excited using a dipole positioned in the silica layer at a radius $r = 40$ nm. (c) Same as (b) but with the resonator excited by a p-polarized plane wave incident along the axial direction, instead of a dipole. In this case, the substrate is not included in the parametrized geometry. The maximum light intensity inside the cavity is 10^4 times the incident light intensity.

of Figure 5a for the 105 nm diameter disk. It clearly shows the ($m = 1$, $n = 1$) nature of the mode. We note that a ($m = 0$, $n = 1$) plasmonic mode also occurs in the spectral range of Figure 4 but is not observed in experiment as it does not couple efficiently to radiation.

The field distribution of the resonant mode was calculated by exciting the resonator (diameter 105 nm, (1,1) resonance at 660 nm) using a dipole source placed in the center of the silica layer at a radius of $r = 40$ nm. By subtracting the dipole field from the calculated local field, we obtain the mode field distribution as is shown in Figure 5b. Similarly, the near field was calculated for a cavity excited by an incoming p-polarized plane wave, as shown in Figure 5c. Both in (b) and (c) we observe a near-field pattern that is very much confined to the silica disk between the two metal particles with the field strongly localized near the cavity edges, which is in agreement with the calculated CL pattern shown as inset in Figure 5a. This is in agreement with what was found for studies of stacked thin metal platelets.[14−16] We note that these very small lowest-order single-mode cavities are identical in nature to the plasmonic hot-spot geometries that are observed in particle dimers.[17,18] Our work thus brings a natural connection between between localized and traveling plasmon cavities.

Next, we study the possibilities for emission control of emitters placed inside the cavity similar to nonresonant metal−dielectric−metal structures.[19,20] From the near-field, we have calculated the mode volume for the resonator,[21] which is found to be $0.00013\lambda_0^3$ or $0.0091\lambda_{SPP}^3$ with λ_0 and λ_{SPP} the free-space and plasmon wavelengths, respectively. The mode volume is 100 times smaller than for typical photonic crystal cavities[22] and more than 1000 times smaller than for typical dielectric disk cavities.[23] Taking into account the theoretical quality factor of $Q = 36$, we find a Purcell enhancement factor of $F_P = 2020$. Using the quality factor $Q = 16$ observed in experiments, a Purcell factor of $F_P = 900$ is expected. This high Purcell factor and the possibility of easily placing emitters in the dielectric layer make these cavities an ideal platform for studies of Purcell-enhanced spontaneous emission and lasing. The Purcell enhancement is observed over a relatively large bandwidth ($Q = 16$), which is a large advantage of these plasmonic cavities over dielectric ones (typically $Q = 10^4-10^8$).

For applications the average Purcell factor for emitters distributed homogeneously inside the dielectric layer might be of interest. We have calculated the average Purcell factor by determining a correction factor from the average of the field inside the SiO_2 layer compared to the maxmium field.[24] We find average Purcell factors of $F_P = 534$ and $F_P = 238$ for calculation and experiment, respectively.

Finally, we have quantified the effect of the chromium layers on the resonator by calculating the scattering cross-section of a resonator only consisting of the Ag/SiO_2/Ag disk, without chromium. The resulting spectrum, also shown in Figure 5a, displays only a slight shift of ~10 nm toward longer wavelengths, at the same Q. This confirms that the presence of the Cr layer has only a minor effect on the cavity resonance.

In conclusion, we have investigated the resonant modes of metal−insulator−metal disk cavities. We have shown that large resonators (diameter 2000 nm, thickness 50 nm) show a broad range of resonances that can be described using a dielectric resonator model using an effective mode index derived from the plasmon dispersion relation. Radial and azimuthal modes are observed and found to be in good agreement with the calculations. Boundary-element simulations reveal the radial and azimuthal mode field distributions. By reducing the resonators diameter to the 65−140 nm range, the lowest-order resonant mode is found in the visible spectral range. A cavity quality factor of $Q = 16$ is found for the 105 nm diameter cavity. The corresponding mode volume is $0.00013\lambda_0^3$, which is 100 times smaller than the smallest mode volume found in photonic crystal cavities and over 1000 times smaller than for dielectric cavities. The resulting Purcell factor is $F_P = 900$ and occurs over a relatively large bandwidth. The high field enhancement inside these MIM disk cavities and their small mode volume makes these ultrasmall disk resonators ideally suited for studies on Purcell-enhanced spontaneous emission and lasing.

Acknowledgment. This work is part of the research program of FOM, which is financially supported by NWO. F.J.G.A. acknowledges support from the Spanish MCeI (MAT2007−66050 and NanoLight.es).

References

(1) Aoki, T.; Dayan, B.; Wilcut, E.; Bowen, W. P.; Parkins, A. S.; Kippenberg, T. J.; Vahala, K. J.; Kimble, H. J. *Nature* **2006**, *443*, 671–674.
(2) Reithmaier, J. P.; Sek, G.; Löffler, A.; Hofmann, C.; Kuhn, S.; Reitzenstein, S.; Keldysh, L. V.; Kulakovskii, V. D.; Reinecke, T. L.; Forchel, A. *Nature* **2004**, *432*, 197–199.
(3) Vahala, K. J. *Nature* **2003**, *424*, 839–846.
(4) Raether, H. *Surface Plasmons on Smooth and Rough Surfaces and on Gratings*; Springer: New York, 1988.
(5) Economou, E. N. *Phys. Rev.* **1969**, *182*, 539–554.
(6) Dionne, J. A.; Sweatlock, L. A.; Atwater, H. A.; Polman, A. *Phys. Rev. B* **2006**, *73*, 035407.
(7) Miyazaki, H. T.; Kurokawa, Y. *Phys. Rev. Lett.* **2006**, *96*, 097401.
(8) Verhagen, E.; Dionne, J. A; Kuipers, L.; Atwater, H. A.; Polman, A. *Nano Lett.* **2008**, *8*, 2925−2929.
(9) Dionne, J. A.; Lezec, H. J.; Atwater, H. A. *Nano Lett.* **2006**, *6*, 1928.
(10) Kuttge, M.; Vesseur, E. J. R.; Koenderink, A. F.; Lezec, H. J.; Atwater, H. A.; García de Abajo, F. J.; Polman, A. *Phys. Rev. B* **2009**, *79*, 113405.
(11) Slusher, R. E.; Levi, A. F. J.; Mohideen, U.; McCall, S. L.; Pearton, S. J.; Logan, R. A. *Appl. Phys. Lett.* **1993**, *63*, 1310–1312.
(12) García de Abajo, F. J.; Howie, A. *Phys. Rev. Lett.* **1998**, *80*, 5180–5183.
(13) García de Abajo, F. J.; Howie, A. *Phys. Rev. B* **2002**, *65*, 115418.
(14) Su, K. H.; Wei, Q. H.; Zhang, X. *Appl. Phys. Lett.* **2006**, *6*, 1928–1930.
(15) Su, K. H.; Durant, S.; Steele, J. M.; Xiong, Y.; Sun, C.; Zhang, X. *J. Phys. Chem. B* **2006**, *110*, 3964–3968.
(16) Dmitirev, A.; Pakzieh, T.; Käll, M.; Sutherland, D. S. *Small* **2007**, *3*, 294–299.
(17) Su, K. H.; Wei, Q. H.; Zhang, X.; Mock, J. J.; Smith, D. R.; Schultz, S. *Nano Lett.* **2003**, *3*, 1087–1090.
(18) Rechtberger, W.; Hohenau, A.; Leitner, A.; Krenn, J. R.; Lamprecht, B.; Aussenegg, F. R. *Opt. Commun.* **2003**, *220*, 137–141.
(19) Jun, Y. C.; Kekatpure, R. D.; White, J. S.; Brongersma, M. L. *Phys. Rev. B.* **2008**, *78*, 153111.
(20) Winter, G.; Murray, W. A.; Wedge, S.; Barnes, W. L. *J. Phys.: Condens. Matter* **2008**, *20*, 304218.
(21) Ruppin, R. *Phys. Lett. A* **2002**, *299*, 309–312.
(22) Noda, S.; Fujita, M.; Asano, T. *Nat. Photonics* **2007**, *1*, 449–458.
(23) Srinivasan, K.; Borselli, M.; Painter, O.; Stintz, A.; Krishna, S. *Opt. Expr.* **2006**, *14*, 1094–1105.
(24) Makarova, M.; Sih, V.; Warga, J.; Li, R.; Dal Negro, L.; Vuckovic, J. *Appl. Phys. Lett.* **2008**, *92*, 161107.

NL902546R